Generation and Validation of a Simulated Radar Ground-Target Database

D. André, D. Blacknell, J. Hare
QinetiQ, St.Andrews Rd, Great Malvern
Worcs. WR14 3PS, UK

DBAndre@QinetiQ.com

ABSTRACT

We generate simulated (I)SAR imagery of a number of ground vehicles with the program Spectre [1] and validate these against turntable (I)SAR imagery from trials. Spectre employs a Physical Optics / Geometrical Optics (PO-GO) or shooting-bouncing-ray high frequency physics model. This approach is employed as standard for high-frequency electromagnetic scattering calculations from large complex bodies, so it is thought that the results have wide relevance. The effects of CAD model complexity and simulation convergence are considered. We evaluate the suitability of the simulated data for use in a database for various kinds of ATR methodologies. There are difficulties in achieving real-time simulations for ATR so we discuss the alternative route of pre-forming a scattering amplitude data-dome for forming monostatic imagery in real-time.

1.0 INTRODUCTION

To form robust Automatic Target Recognition (ATR) algorithms extensive training databases are required. Simulation is seen as a possible route to obtaining a database containing a large variety of imaging scenarios for a wide variety of targets in a wide variety of situations, for a modest cost [2]. The work reported here addresses the generation of a large database of vehicle signature predictions and the comparison of these predictions with real Inverse Synthetic Aperture (ISAR) data for the purposes of validation. The vehicles are modelled ex-situ and are compared with measurements of corresponding vehicles on a Radar Absorbent Material (RAM) covered turntable. The argument in favour of simulation becomes even more favourable if one accepts the point that if the present trend of increasing computer power for a fixed cost continues, it is likely that the possibility of real-time simulation would preclude the need for an imagery database. A database could then consist solely of vehicle Computer Assisted Design (CAD) models which can be articulated by the ATR-simulation software.

The scattering simulation software and the CAD models are discussed in section 2.0. Simulation approximation, convergence and CAD model fidelity dependence have been studied and are described in section 3.0. Detailed feature analysis is described in section 4.0. Validation has been performed through comparison of both simulated and real imagery with the common CAD model to establish that the observed scattering can be jointly associated with structures on the vehicle. Further validation through the use of correlation measures has been undertaken, and is described in section 5.0.

The construction of a database of simulated SAR imagery is greatly facilitated by the pre-calculation of a fully polarimetric K-space representation of the Electromagnetic (EM) scattering. Development of this "datadome" concept to support database generation and image formation research has also been undertaken and is described in section 6.0.

Paper presented at the RTO SET Symposium on "Target Identification and Recognition Using RF Systems", held in Oslo, Norway, 11-13 October 2004, and published in RTO-MP-SET-080.

2.0 FORMATION OF SIMULATED RADAR IMAGERY

2.1 Scattering Software

The EM-simulations were performed for monostatic scattering and a number of runs were carried out at X-band with the QinetiQ prediction code Spectre [1]. The physics models incorporated are the Physical Theory of Diffraction (PTD), the Physical Optics (PO) and Geometrical Optics (GO) approximations [3]. The PO-GO approximation is often called the "shooting-bouncing ray" model. The PTD calculation takes edge effects into account, and PO-GO approximate ray scattering from flat faceted surfaces. In the latter case rays can bounce from a number of surfaces, and if a ray bounces N-times before scattering back to the radar, then this is known as an Nth order scattering effect, or a Multi-Bounce-N event (MB-N). This approach is employed as standard for electromagnetic scattering calculations from large complex bodies at high frequency, so it is thought that our results have wide relevance.

The scattering amplitude as a function of frequency, azimuth and elevation is obtained and is employed to form radar imagery via interpolation, window weighting and the Fourier transform. We have investigated the effects of the various approximations.

2.2 CAD Models

Seven CAD models were obtained for EM-simulation. Here we discuss the T72 main battle tank. These were obtained as part of the CEPA collaboration [4] with three levels of fidelity, to investigate simulation convergence. The low and medium fidelity models in Figure 1 have 9611 and 24808 facets respectively. The high fidelity model in Figure 2 has 37701 facets. Note that both the medium and high fidelity T72 models have high fidelity wheels and tracks but that the low fidelity model does not. At high radar frequency we find this affects the scattering properties a great deal and, in particular, the convergence of scattering amplitude as a function of multi-bounce order.

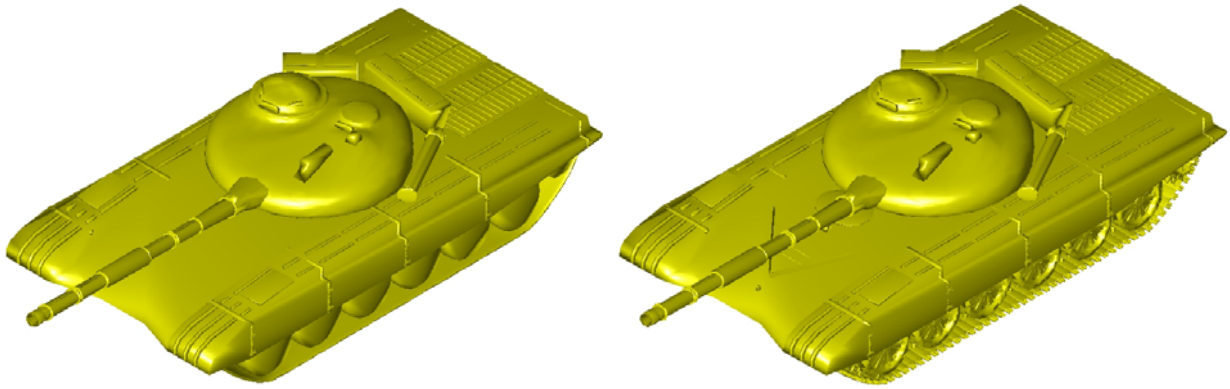

Figure 1: T72 CAD models. Left: low level of fidelity with 5307 vertices and 9611 faces. Right: medium fidelity model with 21561 vertices and 24808 faces. The low fidelity model has highly simplified tracks and wheels.

3.0 APPROXIMATION AND CONVERGENCE

3.1 Reciprocity

Polarimetric radars can transmit and receive two orthogonal polarisations. In the linearly polarised case the polarisations are labelled H for horizontal and V for vertical. In this way four transmit-receive combinations are possible (HH, HV, VH and VV). This additional data allows a more detailed examination of the scattering mechanisms.

The results from Spectre are generally not reciprocal. In the monostatic case this implies that HV simulation results erroneously differ from the VH results. This is not the case in reality. This is due to a failing of high frequency approximation physical models. The PO approximation is not reciprocal [5] and this problem is further exacerbated by having to employ PO-GO. This is where in order-N interactions, the first N-1 are modelled with GO reflections and only the last interaction is modelled with PO scattering. This is a standard high frequency modelling technique. For complex bodies there is very little alternative to applying PO-GO given the exponential increase in required computing power with scattering interaction order, which would occur for full PO scattering prediction.

3.2 Further Numerical Approximations

Beyond the underlying high-frequency ray-tracing approximation upon which the Spectre physics model is based, and the fact that the CAD-model is also approximated, other approximations were employed to reduce the computational run-time. Among these was a frequency sweep approximation. Here the fundamental scattering amplitude of any given facet is assumed to remain independent of frequency so that all variation within the band is solely due to the ray-path length difference in units of wavelength, and due to interference between scatterers as a result of this. This is found to be a very good approximation at HF. Various other approximations were employed, including an azimuth interpolation and a truncation of the scattering when it is away from the specular reflection direction by more than 30º. These are described in [6].

3.3 Convergence

Simulated radar imagery results for the low and medium fidelity T72 models were decomposed into pure edge diffraction contributions and pure N-bounce ray components [1][3][6]. This was done to help understand the origin of features and to estimate whether the imagery has converged as a function of increasing ray-bounce. The imagery has a resolution of 10cm. In Table 1 we see how the simulated imagery for the low fidelity model converges reasonably well by MB-4. The tables show imagery in the two polarization channels HH and HV. The rows 1-3 in Table 1 show increasing MB components from order 4 to order 6. The bottom row consists of all the components added together coherently. We see that very few dim scattering centres are apparent for the MB-4 events image (NB: the colour-scale is reset in each image). The same cannot be said for the medium fidelity T72 for which the corresponding component can be found in Table 2. We see that convergence is not achieved. This is due to the higher complexity of the wheels and tracks on this model (see Figure 1). However the sum-total images are more realistic than in the lower fidelity simulation in that the wheels and tracks are now much more prominent than in the imagery for the low fidelity model (see for example [7]).

Investigation has shown that for the medium and high fidelity models, for some aspect angles back scattering only reduced considerably after 5 or 6 bounces. Because of the complex nature of the high fidelity targets, some features may remain bright for even higher bounces, possibly with no convergence as a function of multibounce. This can certainly be the case for general cavity back-scattering [8][9]. Furthermore, in a complex target, even after we have seemingly obtained convergence with MB-N0, where N0 is any positive integer, we could never be sure that there would not occur a bright response at MB-N, where N>N0. Indeed we could purposefully contrive a simple target consisting of N mirrors, and seemingly obtain what looks like convergence with MB-N0 where N0<N, and yet if we have arranged the mirrors correctly, have a very bright response at MB-N. This could be done for any positive integer N.

For the simulated image database we have settled for the combination of diffraction and multibounce up to and including third order scattering events (MB-3). Higher order events were not calculated due to the computational cost involved in calculating the full azimuthal dataset over the full 360º.

Table 1: Simulation multibounce (MB-N PO) component and sum-total images, showing convergence of scattering response with increasing multibounce, for the low fidelity T72 in the polarization channels HH and HV. The bottom row shows all components added together coherently. Resolution is 10cm (NB: the colour-scale is reset in each image).

	HH	HV
MB-4 PO	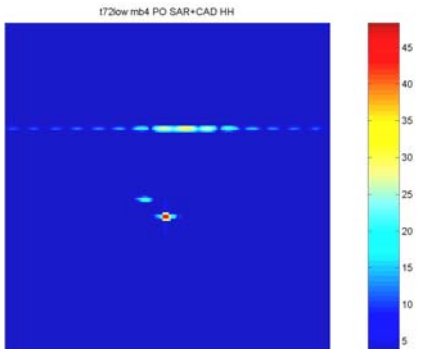	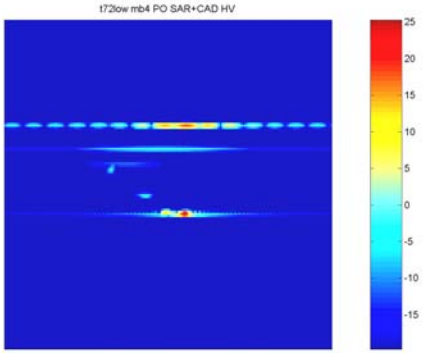
MB-5 PO	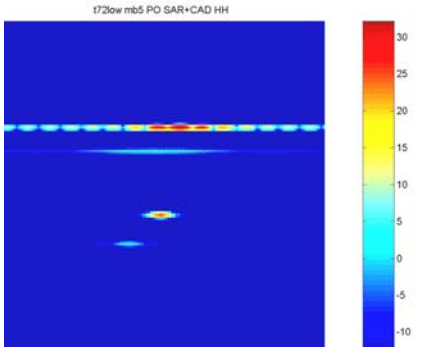	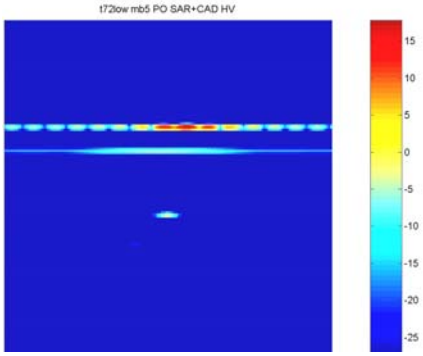
MB-6 PO	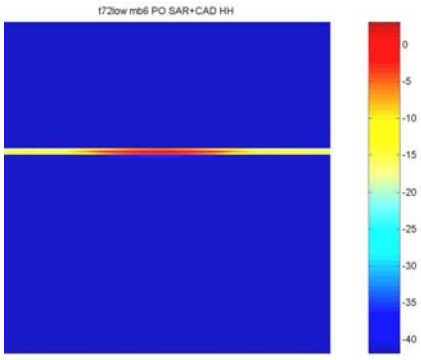	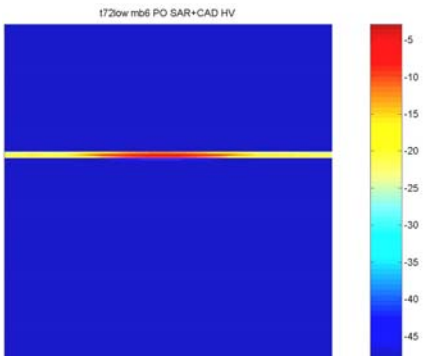
MB-1+2+…+6 PO + PTD	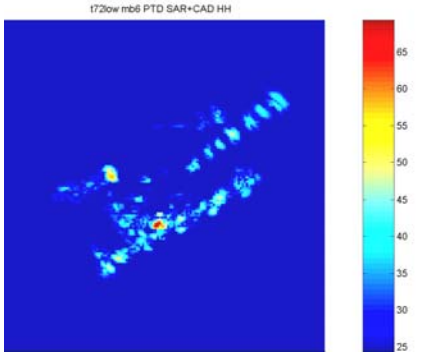	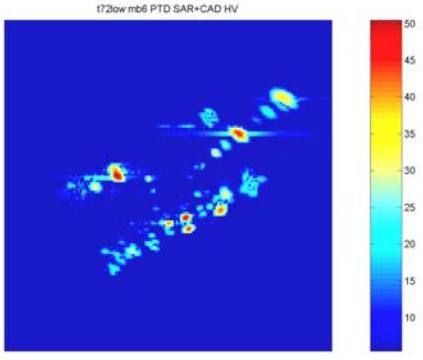

Table 2: Simulation multibounce (MB-N PO) components and sum-total images, showing convergence of scattering response with increasing multibounce, for the medium fidelity T72 in the polarization channels HH and HV. The bottom row shows all components added together coherently. Resolution is 10cm (NB: the colour-scale is reset in each image).

	HH	HV
MB-4 PO	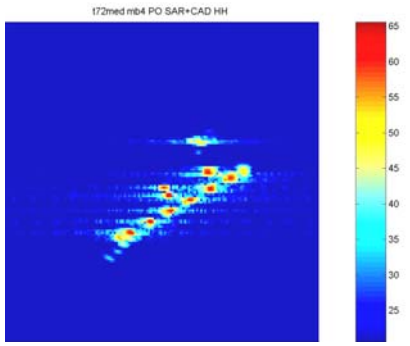	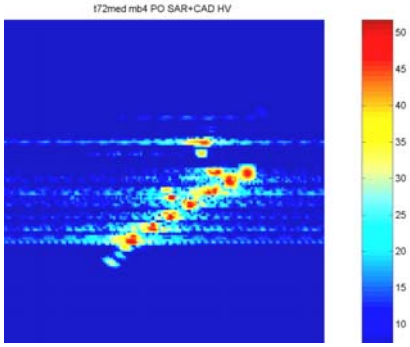
MB-5 PO	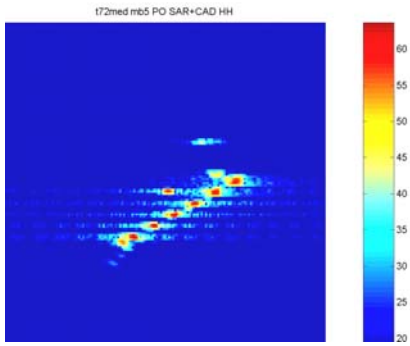	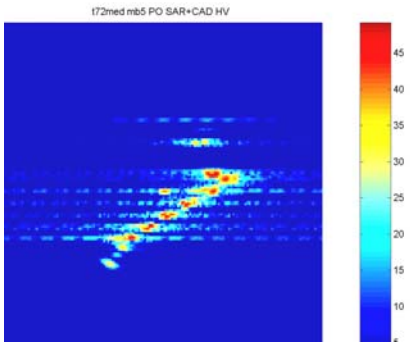
MB-6 PO	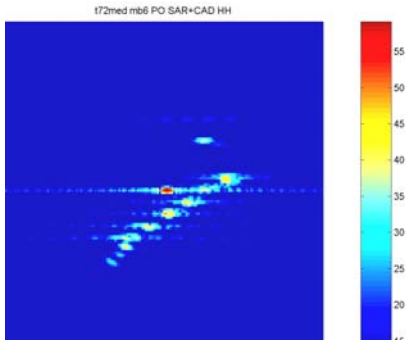	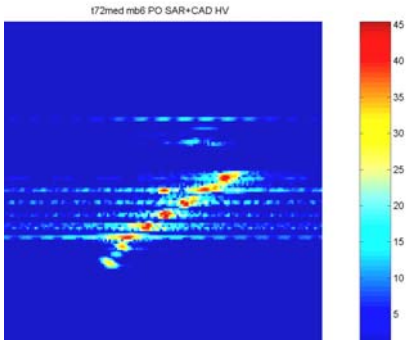
MB-1+2+…+6 PO + PTD	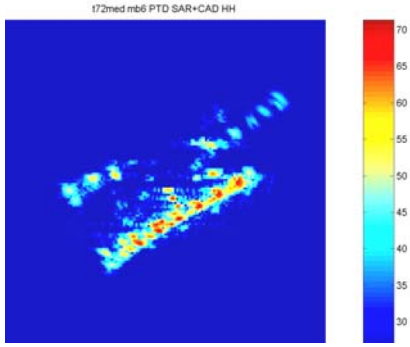	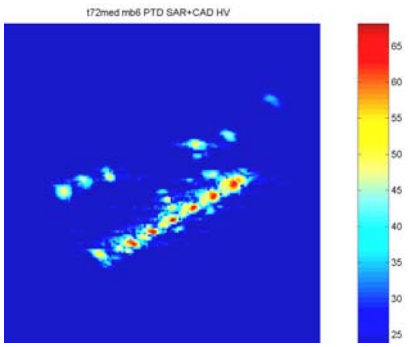

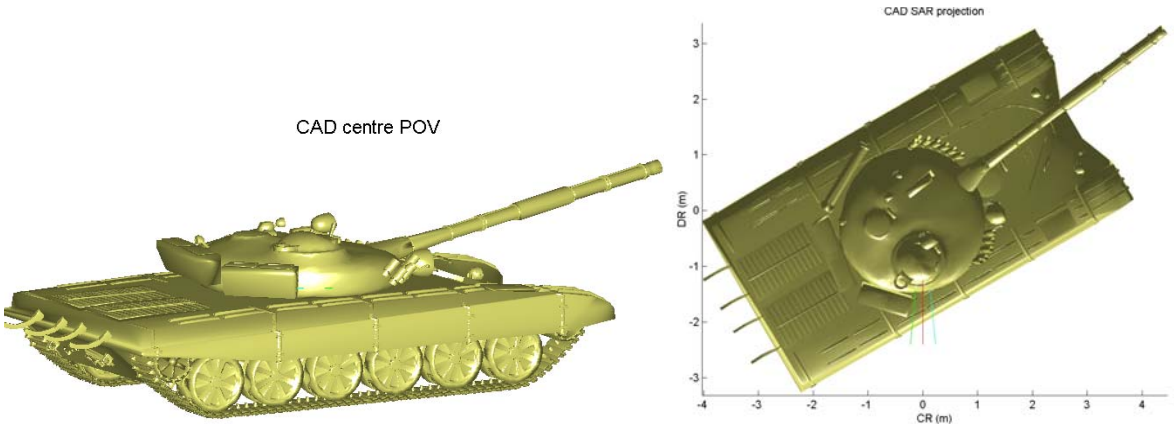

Figure 2, Left: High fidelity T72 Radar Point of View (POV) in the centre of the azimuthal imaging aperture used to form the radar imagery portrayed in Figure 3. Azimuth angle az=120° and elevation el=10°. Right: High fidelity T72 projection corresponding to that in Figure 3. The extent of the azimuthal imaging aperture is portrayed with the green and blue lines, and that the red line corresponds to the central POV. This aperture is required for the formation of 10cm resolution imagery at X-band. The illumination on the model is from the intended radar direction, thus giving an indication of the location of possible scattering hot-spots.

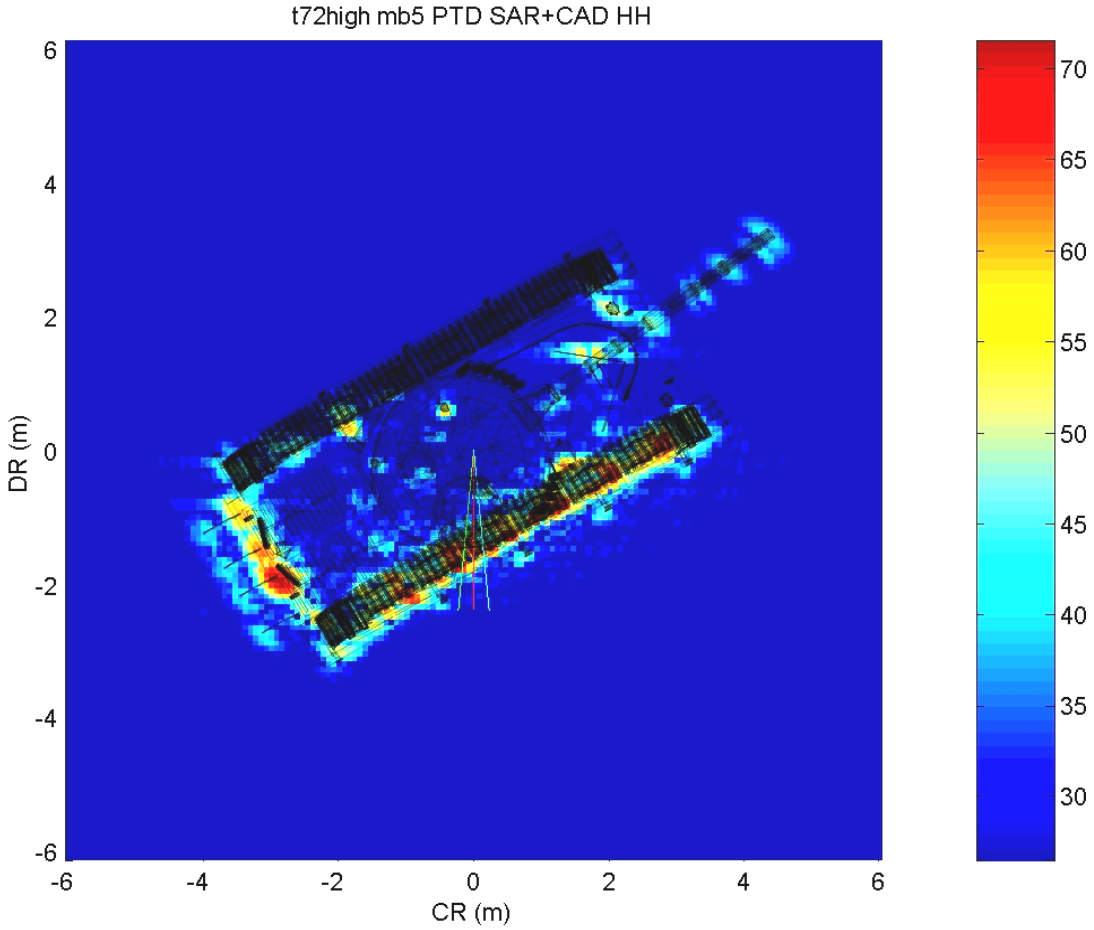

Figure 3: Diffraction plus multibounce up to order 5 (PTD + MB-1 +… MB-5) simulated radar image of high fidelity T72 with CAD wire-frame superimposed. Three lines represent radar POV azimuth aperture extent and centre.

4.0 FEATURE ANALYSIS

A feature analysis was carried out consisting of overlaying a partially transparent CAD wire-frame model onto the corresponding radar image, and comparing with radar Point of View (POV) CAD projections. This has greatly helped us to identify radar scattering hot-spots, their origins and their subsequent scattering centres in the imagery.

In Figure 2 on the left we see the high fidelity T72 central POV CAD projection corresponding to the radar image in Figure 3. In Figure 2 on the right we see the CAD projection corresponding to that in the associated radar image. A partially transparent projection of the wireframe is superposed onto the radar image and we can see how well they correspond. Note that this latter projection is not a top projection, but is at 10º from the vertical in the appropriate direction. This is because the radar elevation is at 10º. This distinction seems small here, but helps to explain the minutiae of overlay effects. The distinction becomes crucial for higher elevation angle imagery interpretation. We note that the track and wheel scattering responses are not in a straight line, but are slightly arced in the radar imagery. This is a layover effect which is readily understood through application of the wireframe overlay.

Note that the extent of the azimuthal imaging aperture is portrayed with the green and blue lines both in the radar image and in the corresponding CAD projection (Figure 2, right). The red lines correspond to the central POV, and the green and blue lines correspond to the azimuth aperture extent limits (necessary for 10cm resolution). Analysis of the variation of POV within a single image has helped us to identify unstable scatterers. For example those which become obscured during part of an aperture. Scattering centres which correspond to unstable scatterers lead to cross-range smearing. An example is provided by the wheel to the rear and left of the T72. Note that the imaging geometry described here was also employed in the formation of the imagery in Table 1 and Table 2.

The feature analysis was carried out both for simulated and trials imagery of various vehicles at 30cm resolution. Generally the corresponding scatterer locations were found to have been predicted correctly, however often the predicted brightness of these scattering centres was incorrect. This type of observation and others like it guide the appropriate choice of feature extraction algorithm to be applied in simulated database ATR. In the following section we do not describe feature extraction procedures, but merely apply normalised image correlations between real and simulated datasets and discuss results.

5.0 CORRELATION OF SIMULATED AND TRIALS ISAR IMAGERY

5.1 Correlation Procedure

Here we describe the results of correlating the simulated and the trials imagery. Before correlating, the polarimetric span was taken

$$Span = \sqrt{|HH|^2 + 2|HV|^2 + |VV|^2} \qquad \text{Equation 1}$$

where *HH*, *HV* and *VV* are the images in these respective polarimetric channels and the sum is carried out on a pixel-by-pixel basis. Taking the span generally gave rise to more consistent correlation results. Next the images were normalized as follows: the mean was subtracted and the result was divided by the standard deviation. For the image F, the normalized image F_n is

$$F_n(i,j) = \frac{F(i,j) - \overline{F}}{\sqrt{\sum_{i'}\sum_{j'}\left[F(i',j') - \overline{F}\right]^2}} \qquad \text{Equation 2}$$

where the over-bar indicates the mean value of the image.

Depending on the goal one wishes to achieve, one may scale the images in different ways. For example to enhance the bright peaks, one could square the images, or to bring out the overall structure one could take the square root of the image, or take the logarithm. Prior to normalizing the images we have chosen to take the logarithm and to take a threshold from below at 45dBm^2 from the image maximum value. This is not appropriate for some types of imagery and this depends upon the noise threshold amongst other things.

The image correlation C is defined as follows

$$C(i,j) = \sum_{i'} \sum_{j'} f(i',j')\, g(i'-i, j'-j) = IFT\left[F\, conj(G)\right] \qquad \text{Equation 3}$$

where f and g are the images to be correlated, F and G are their Fourier transforms, IFT[·] is the inverse Fourier transform and $conj(\cdot)$ is the complex conjugate. Because the images have been normalized, the values of C vary only from 0 to 1. From the correlation image C one can extract the maximum correlation, and its position, which indicates to where one of the images should be shifted for the best template match.

5.2 Correlation Results

Polarimetrically-calibrated X-band turntable trials imagery at 30cm of a military vehicle was obtained. The corresponding CAD model was at very high fidelity, with just under 100000 facets. Even though the model was at high fidelity, it was still noticeable that particular details did not match. We should note however that this is also the case between different real vehicles of the same type. We are forced to take the view that any robust ATR algorithm must compensate for this inherent variation. The database for each consisted of 360 images at 1° intervals in all polarisations. The simulations only took into account edge diffraction and first to third order multibounce interactions. Due to run-time considerations no higher interactions were calculated here.

In Figure 4 on the left we see maximum correlation results between the experimental and numerical imagery of vehicle 1 as a function of aspect angle. The average correlation is about 0.8. On the right of Figure 4 we see the shift distance of image 1 for maximum correlation with image 2. This distance roughly follows a cosine curve which simply reflects the fact that the centre of rotation of the trials vehicle is not exactly collocated with that of the simulated vehicle.

In Figure 5 we see maximum correlation results between the experimental vehicle 1 dataset and a simulated vehicle 2 dataset. The average correlation decreased to about 0.7, which is lower than for the same type vehicle case. Although we indeed find that correlations are now lower, the difference is only around 0.1. We conclude that simple template matching is not sufficient to make optimal use of simulated imagery databases. It is likely that feature extraction based on scatterer position may be a better approach. In Figure 5 on the right, we see the template shift for maximum correlation. We see that a sinusoid of the appropriate period can no longer be fitted, supporting the conclusion that the vehicles being matched are of different types.

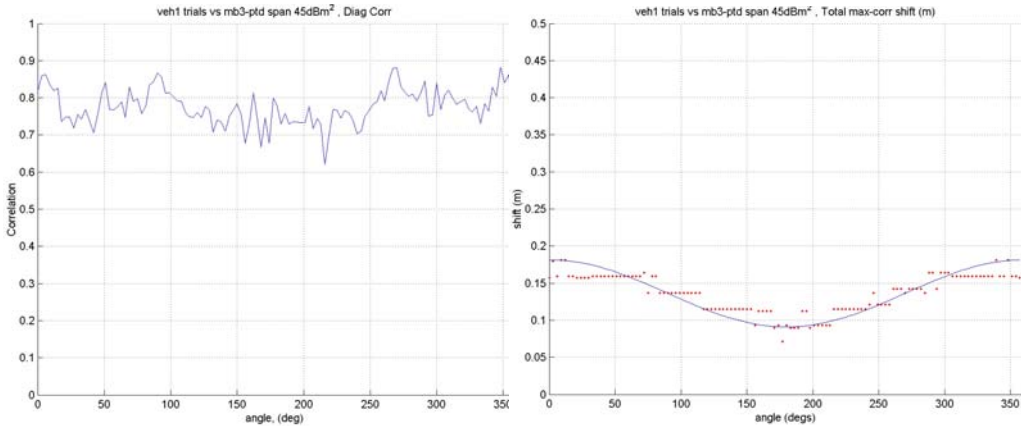

Figure 4, Left: Equal-angles maximum correlations as a function of azimuth (equal aspect image. Right: Template shift distance to maximum correlation for equal aspect image comparisons. The points follow a sinusoid.

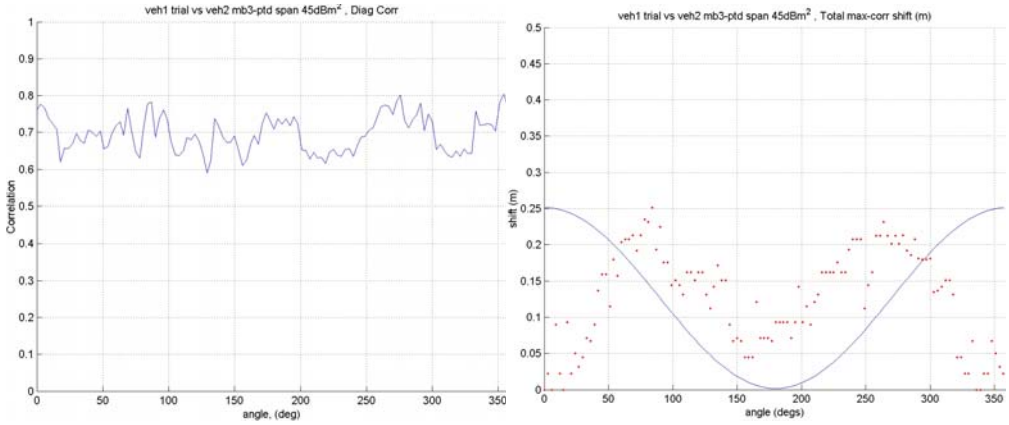

Figure 5, Left: Equal-angles maximum correlations as a function of azimuth (equal aspect image comparisons). Right: Template shift distance to maximum correlation for equal aspect image comparisons. The points do not follow a sinusoid with the expected period.

6.0 SCATTERING AMPLITUDE DATADOME

The practicality of avoiding the need to generate large databases of simulated imagery for many possible imaging geometries and platform trajectories can be addressed by the introduction of the "data-dome" concept.

In constructing an image database for ATR, various factors such as the introduction of radar resolution as a variable, or the "angle of squint" variable in SAR squint mode imaging can have a drastic impact on the size of the image database. Clearly there are many other factors which can have a significant impact on imagery and these include elevation angle, centre frequency of image support, pixel spacing, windowing type for side-lobe suppression to name but a few. For this reason we argue the case for the pre-calculation of a frequency wide-band fully polarimetric scattering amplitude data-dome, which can be employed in forming imagery to the exact required specifications quickly. The other point is that potentially, the imagery can be formed with the data-dome in real-time.

The scattering amplitude datadome is a K-space or Fourier domain spherical shell of scattering amplitude values. Frequency is represented as distance from the origin and both azimuth and elevation in this space represent the radar-pulse direction towards the target azimuth and elevation angles. If one requires say a maximum of 5cm resolution for a ground vehicle, such a data-dome can be voluminous and can occupy storage space of the order of 90Gb. However this quantity easily fits onto a single modern, fast and inexpensive hard-disk.

We have formed such data-domes for simple test objects, consisting of collections of cubes however it was soon realised that forming a high resolution data-dome for a large ground target would be highly non-trivial in terms of computational expense. To continue our preliminary investigation we have obtained an unclassified datadome corresponding to a civilian digger vehicle (JCB or Backhoe), known as the "Backhoe datadome" [10]. This data was created with the simulation tool X-Patch [11]. This software also employs the high-frequency PO-GO approximation. The data has a frequency bandwidth of 6GHz with a centre frequency of 10GHz and an angular sampling in azimuth and elevation of 0.07°. The data-dome allows very high resolution imaging, potentially down to 3cm, for a target of about 15m in length.

Initial investigations have shown that 2-D image formation from such a dome is rapid and provides a feasible way forward to overcoming the present inability to perform scattering predictions in real-time. Clearly, for complex targets this is the case because simulation run-time is simply replaced by data retrieval-time plus data interpolation-time. Specifically, if the data dome is stored upon a fast data access medium and if the target CAD model is of a medium to high level of fidelity, then the ratio of simulation run-time plus image formation time, to data-dome data retrieval plus data-interpolation plus image formation time, may be of the order of 1000. This is certainly the case if high resolutions are required.

Due to the ease in obtaining the Fourier domain image support, the data-dome approach has allowed us to perform timely investigations of non-trivial effects such as varying overlay, lighting, obscuration and multipath effects in 2-D imagery. These should all be thoroughly understood to allow the formation of an effective ATR template matching scheme. Further studies of 3-D radar image formation were also undertaken with relative ease.

7.0 CONCLUSION

Our ISAR image comparisons consisting of feature analysis and correlation have shown that simulated imagery is broadly similar to trials imagery, although there are always specific differences. Scattering centres generally exhibit different relative brightnesses and additionally trials imagery is subject to the appearance of random scatterers. These differences are partly due to differences between the CAD models and the real vehicles, and also due to the high-frequency scattering approximations implemented. One can go on to argue that the differences are partly due to environmental effects and to inherent instabilities in the equipment. Additionally real vehicle surface roughness and coatings affect EM-responses. Although in the trials Radar Absorbent Material (RAM) coatings were employed on the turntable surface, there are still likely to be significant multi-path ground interactions, due to the turntable base disk being neither large enough nor perfect enough.

There is of course always some variation between the vehicles of the same class, which cannot be accounted for in any one CAD model. For example on the day of the trials some of the cam baskets were filled or covered, some of the wing-mirrors were in position, others not. The periscope mirrors were at different orientations, and of course the tracks and wheels could never be deployed in any exact way. One could not for example expect even trials imagery of the same vehicle, taken on different days to be the same [12].

Many approximations are carried out for the EM-simulations. We have described some of these approximations, convergence issues and even the effect of employing different CAD fidelities. It was found that higher detailed wheels and tracks give more realistic imagery, however they are less likely to converge as a function of ray-bounce.

From our detailed feature analysis we have come to the conclusion that we are able to predict the location of prominent scatterers, although they are often of a brightness different to that seen in actual trials imagery. It is our opinion that for successful ATR we will need to extract robust and prominent features automatically and we will need to emphasise the positional information over the brightness information. This work is ongoing and we have not been discouraged by our results. It may well be the case that converged EM-simulation (which are often not possible [7][8][9]) may not be required for ATR.

Data-dome studies have shown that tailored image formation is extremely rapid, sometimes of the order of 1000 times more rapid, depending upon the specific situation, when compared to the time taken for simulation plus image formation. For example, the specific relative speed would depend upon CAD model complexity, the simulation approximations employed and on the required resolution. We can see that this must be the case because simulation run-time is simply replaced by data-retrieval followed by data-interpolation time.

All possible imagery databases for a given target could be replaced by a data-dome with a suitable image formation algorithm. For example, for ATR using a database of pre-formed imagery one must be careful to employ the appropriate image database to the corresponding imagery. For example, in squinted imagery it can be shown that layover always occurs in one direction for images formed with data from any part of a straight radar platform track, whereas for ISAR imagery it always occurs towards the imaging platform instead. For a broadside elevation angle of more than 20° this difference can be clearly seen, when comparing images from equal illumination directions.

In the case of wide-aperture imaging, which is required for high resolution SAR and even more-so at low frequency bands, ISAR and SAR can also be very different at such elevations. This is because, whereas in ISAR imaging the elevation angle remains constant, in the case of SAR, the elevation angle is actually changing along the course of the aperture. Thus in the case of complex target imaging where scattering amplitude can change considerable for small elevation angle changes, the image type itself (SAR, ISAR, Squint mode SAR) can have a large impact on the imagery. The availability of a data-dome allows one to accommodate all these imaging scenarios in real time and can also reduce the overall size of an ATR database.

8.0 ACKNOWLEDGEMENT

This work was sponsored by the Electronic Systems domain of the UK MOD Corporate Research Program.

9.0 REFERENCES

[1] Spectre (formally known as RESPECT). S.D.Turner, *RESPECT: Rapid Electromagnetic Scattering Predictor for Extremely Complex Targets*, Radar and Signal Processing, IEE Proceedings F, Volume: 137, Issue: 4l

[2] Hummel R. *Model-Based ATR Using Synthetic Aperture Radar*, IEE International Radar Conference, 7-12May 2000, pp856-861.

[3] Knott E, *Radar Cross Section,* 2nd edition, Artech House 1993.

[4] CEPA: Supplement No JP 1.18 to the WEAG Memorandum of Understanding for Technology Arrangement for Laboratories for Defence European Science (Thales), concerning Target and Target Background Modelling Validation for High-Resolution Radar. July 2002.

[5] Ulaby F. *Radar Polarimetry for Geoscience Application*, Artech House 1990.

[6] Turner S. *Spectre user guide,* Unpublished QinetiQ Report.

[7] Rihaczek A. *Theory and Practice of Radar Target Identification*, Artech House 2000.

[8] MacKay A. *An Application of Chaos Theory to Ray Tracing in Ducts*, Unpublished DERA report.

[9] Smilansky U. *Chaotic Scattering of Microwaves*, Journal of Radio Science, Sept 2001.

[10] Backhoe Sample Public Release Visual-D Challenge Problem, http://www.sdms.afrl.af.mil/main.htm

[11] X-Patch, http://www.saic.com/products/software/xpatch

[12] Bennett A. *The Stability of Polarimetric Features for Target Classification From SAR Imagery*, IEE RADAR2002 conference publication, No.490, pp395-9.